# Seismic Wavelet Estimation Using Covariation Approach

Bibo Yue, Zhenming Peng, *Member, IEEE*, and Qiheng Zhang

***Abstract*—This paper proposes a novel covariation approach for seismic wavelet estimation under the assumption that a real seismic signal follows non-Gaussian $\alpha$-stable distributions. Since the non-Gaussian $\alpha$-stable signals do not have finite second or higher order moments, the traditional methods of Gaussian distribution may not get a suitable solution. Based on the principle of fractional lower order statistics, the covariation approach deconvolution objective function matrix was given, and the details of wavelet estimation with the covariation approach were presented. Furthermore, computer simulation experiments on theoretical synthetic data and real seismic data were conducted. In the experiments, the effect of moments was considered. Among the estimated wavelets with different moments, the best wavelet should be the one with moment less than characteristic but close to characteristic. To verify the correctness and effectiveness of the proposed method, the extracted real wavelet was applied in real seismic acoustic impedance inversion. The result from the inversion of the 2-D real data set is consistent with the well log interpretation very well.**

***Index Terms*—Covariation, fractional lower order statistics, seismic wavelet estimation, $\alpha$-stable distribution.**

## I. Introduction

SEISMIC wavelet estimation plays an important role in seismic inversion and reservoir characterization studies. Standard wavelet estimation and seismic signal processing techniques assume that the seismic signals follow Gaussian distribution [1], based on which a great deal of estimation methods has been proposed [2]–[6]. However, many scholars have pointed out that the seismic signals do not follow Gauss distribution generally and have proposed many non-Gaussian distribution models, e.g., Walden [7] modeled the reflectivity coefficient amplitude distribution by generalized Gaussian, and Godfrey [8] chose the generalized Cauchy distribution as empirical distribution about the reflectivity coefficient. Yue [9] studied the heavy tailed character of seismic signals and proposed that the real seismic signals follow non-Gaussian $\alpha$-stable distributions.

Manuscript received June 5, 2013; revised September 8, 2013 and December 3, 2013; accepted February 18, 2014. This work was supported by the National Natural Science Foundation of China under Grants 41274127, 40874066, and 40839905 and by the Fundamental Research Funds for the Central Universities under Grant ZYGX2011YB021.

B. Yue and Z. Peng are with the School of Opto-Electronic Information, University of Electronic Science and Technology of China, Chengdu 610054, China (e-mail: yuebibo@gmail.com; zmpeng@uestc.edu.cn).

Q. Zhang is with the Institute of Optics and Electronics, China Academy of Sciences, Chengdu 610209, China (e-mail: qhzhang@ioe.ac.cn).

Color versions of one or more of the figures in this paper are available online at http://ieeexplore.ieee.org.

Digital Object Identifier 10.1109/TGRS.2014.2313116

$\alpha$-stable distributions are a rich class of distributions that include the Gaussian and Caution distribution in a family that allows skewness and heavy tails [10], [11]. Hence, $\alpha$-stable distributions are more feasible than Gaussian distribution. Since characterized by Paul Lévy in his study of sums of independent identically distribution terms in the 1925, a vast amount of knowledge has been accumulated about the properties of the $\alpha$-stable distributions, and they are applied in the field of signal processing since Nikias and Shao's work [10], [11]. Recent advances on this subject have been made in communication [12], identification [13], array signal processing [14], and so on. Since non-Gaussian $\alpha$-stable distributions do not have finite second or higher order moments, traditional mean square or high-order statistics processing methods may not lead to a suitable solution, and the fractional lower order moment (FLOM) is applied instead. The covariation is a kind of FLOM, and it plays a role analogous to covariance in Gaussian case. Since Gaussian distribution is a special case of $\alpha$-stable distributions, the covariation algorithm is robust for both Gaussian and non-Gaussian $\alpha$-stable distributions.

This paper follows the assumption that a real seismic signal is a non-Gaussian $\alpha$-stable distribution [9] and proposes a new wavelet estimation method by using covariation. The rest of this paper is organized as follows. In Section II, some necessary preliminaries on $\alpha$-stable distribution and covariation are presented. In Section III, wavelet estimation by using covariation approach is formulated. Finally, in Section IV, simulation experiments are conducted on synthetic data and real seismic trace; the results verify the correctness and effectiveness of the proposed wavelet estimation.

## II. Mathematical Preliminaries

Since most of the $\alpha$-stable distributions do not have closed-form probability density functions, except for a few known cases, they are conveniently described by the characteristic function. For a given $\alpha$-stable random variable, named X, it has a characteristic function

$$\varphi(u) = \exp\left\{j\mu u - \gamma|u|^{\alpha}\left[1 + j\beta \mathrm{sgn}(u)\omega(u,\alpha)\right]\right\} \tag{1}$$

where

$$\omega(u,\alpha) = \begin{cases} \tan\left(\frac{\pi\alpha}{2}\right), & \alpha \neq 1 \\ \left(\frac{2}{\pi}\right)\log|u|, & \alpha = 1 \end{cases} \tag{2}$$

$$\mathrm{sgn}(u) = \begin{cases} 1, & u > 0 \\ 0, & u = 0 \\ -1, & u < 0. \end{cases} \tag{3}$$

The $\alpha$-stable characteristic function is completely determined by four parameters, namely, $\alpha$, $\beta$, $\gamma$, and $\mu$. $\alpha(0<\alpha\leq 2)$ is the characteristic exponent; the smaller the value of $\alpha$, the heavier tails the stable distributions will have. $\beta(-1 \leq \beta \leq 1)$ is the symmetry parameter, and when $\beta = 0$, the distribution will be symmetric $\alpha$-stable ($S\alpha S$) distributions. $\gamma(\gamma > 0)$ is the dispersion, and $\mu(-\infty < \mu < \infty)$ is the location parameter.

Due to the thick tails, $\alpha$-stable distributions do not have finite second or higher order moments, except for the limiting cases $\alpha = 1$ and $\alpha = 2$. For a non-Gaussian $\alpha$-stable distribution with characteristic exponent $\alpha$, only moments of order less than $\alpha$ are finite, called FLOM. The FLOM for an $S\alpha S$ random variable $X$ is [10]

$$E\left(|X|^p\right) = C(p,\alpha)\gamma^{p/\alpha} \qquad 0 < p < \alpha \leq 2 \tag{4}$$

where $C(p,\alpha) = 2^{p+1}\Gamma((p+1)/2)\Gamma(-(p/\alpha))/\alpha\sqrt{\pi}(-(p/2))$ and $\Gamma(x) = \int_0^\infty t^{x-1}e^{-t}dt$. However, for $0 < \alpha < 2$, $E(|X|^p) = \infty$ if $p \geq \alpha$.

For two jointly $S\alpha S$ random variables $X$ and $Y$ with $1 < \alpha < 2$, the covariation is defined as

$$[X,Y]_\alpha = \int_S xy^{\langle\alpha-1\rangle}\mu(ds) \tag{5}$$

where $S$ is the unit circle, $\mu(\bullet)$ is the spectral measure of the $S\alpha S$ random vector $(X,Y)$, and convention $Y^{\langle p\rangle} = |Y|^{\langle p\rangle}sign(Y)$ for any real or complex $Y$. Although it is different to obtain covariation based on the definition, the covariation [10]–[16] can be computed using the FLOM given by

$$[X,Y]_\alpha = \frac{E\left(XY^{\langle p-1\rangle}\right)}{E\left(|Y|^p\right)}\gamma_Y, \quad 1 \leq p < \alpha \tag{6}$$

where $\gamma_Y$ is the dispersion of the random vector $Y$ given by

$$\gamma_Y^{p/\alpha} = \frac{E\left(|Y|^p\right)}{C(p,\alpha)}, \quad \text{for} \quad 0 < p < \alpha. \tag{7}$$

Obviously, from (6), it holds that

$$[X,X]_\alpha = \gamma_X \tag{8}$$

Also, the covariation coefficient of $X$ and $Y$ is defined by

$$\lambda_{X,Y} = \frac{[X,Y]_\alpha}{[Y,Y]_\alpha}. \tag{9}$$

Moreover, by using (6), it can be expressed as

$$\lambda_{X,Y} = \frac{E\left(XY^{\langle p-1\rangle}\right)}{E\left(|Y|^p\right)}, \quad \text{for} \quad 1 \leq p < \alpha. \tag{10}$$

Several useful properties of covariation are given as follows.

*Property 1:* The covariation $[X,Y]_\alpha$ is linear in $X$: If $X_1$, $X_2$, and $Y$ are jointly $S\alpha S$, then

$$[AX_1 + BX_2, Y]_\alpha = A[X_1,Y]_\alpha + B[X_2,Y]_\alpha \tag{11}$$

for any real constants $A$ and $B$.

*Property 2:* The covariation $[X,Y]_\alpha$ is a pseudolinearity property with respect to $Y$: If $Y_1$ and $Y_2$ are independent and $Y_1$, $Y_2$, and $X$ are jointly $S\alpha S$, then

$$[X, AY_1 + BY_2]_\alpha = A^{\langle\alpha-1\rangle}[X,Y_1]_\alpha + B^{\langle\alpha-1\rangle}[X,Y_2]_\alpha \tag{12}$$

for any real constants $A$ and $B$.

*Property 3:* If $X$ and $Y$ are independent and jointly $S\alpha S$, then

$$[X,Y]_\alpha = 0.$$

## III. Seismic Wavelet Estimation With Covariation

The seismic wavelet is a required input to many seismic processing, modeling, and inversion application, and no specified wavelet may lead to erroneous results [17]. The wavelet estimation methods fall into two main classes depending on whether well log information is used or not. Generally speaking, the wavelet estimation methods by using well log information would obtain better wavelet than the ones without well log information. In this paper, the wavelet is estimated from seismic and well log data, involving solving a set of equations relating the reflectivity coefficients to the seismic trace. In seismology, the recorded seismic trace $s(t)$ is defined to be the linear convolution of the source wavelet $w(t)$ with the reflectivity coefficients $r(t)$; thus, the convolution model may be written as [18]

$$s(t) = w(t) * r(t). \tag{13}$$

Therefore, the discrete representation of (13) is given as

$$s(i) = \sum_{j=1}^{M} w(i,j)r(j), \quad j = 1,2,\ldots,M. \tag{14}$$

In this paper, we believe the assumption that the seismic signal is $S\alpha S$ because the signal is of infinite variance [9]. Covariation of two random processing $s(n)$ and $r(n)$ is defined as [19], [20]

$$\begin{aligned} R_{s,r}(m) &= E\left\{s(n)\left[r(n+m)\right]^{\langle p-1\rangle}\right\} \\ &= E\left\{s(n)\left|r(n+m)\right|^{p-1} sign\left[r(n+m)\right]\right\} \end{aligned} \tag{15}$$

where $1 \leq p < \alpha$.

Given seismic trace $\mathbf{s}$ and reflectivity coefficient $\mathbf{r}$, the covariation is estimated by the sample covariation

$$\tilde{R}_{s,r}(m) = \frac{1}{N}\sum_{n=1}^{N} s(n)\left|r(n+m)\right|^{p-1} sign\left(r(n+m)\right). \tag{16}$$

According to (14), we obtain the following expression for the covariation of seismic trace $\mathbf{s}$ and reflectivity coefficients $\mathbf{r}$

$$E\left[s(i)r(l)^{\langle p-1\rangle}\right] = E\left[\left(\sum_{j=1}^{M} w(i,j)r(j)\right)r(l)^{\langle p-1\rangle}\right], \quad l = 1,2,\ldots,M. \tag{17}$$

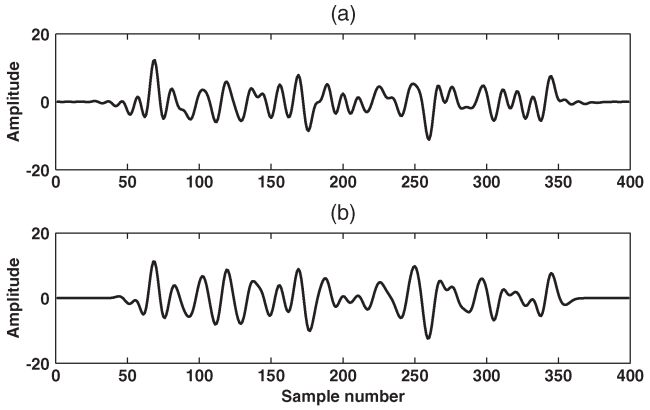


Fig. 1. Synthetic traces for wavelet estimation. (a) Generated by convolving a normalized $S\alpha S$ pseudoreflectivity coefficient with a bandpass wavelet. (b) Generated by convolving a normalized $S\alpha S$ pseudoreflectivity coefficient with a Ricker wavelet.

Combining (16) and (17), we can obtain the following expression:

$$\mathbf{\Gamma_{sr}} = \mathbf{\Gamma_r}\mathbf{w} \tag{18}$$

where $\mathbf{\Gamma_{sr}} = [R_{s,r}(1), R_{s,r}(2), \cdots, R_{s,r}(M)]^T$, $\mathbf{w} = [w(1), w(2), \cdots w(M)]^T$, and

$$\mathbf{\Gamma_r} = \begin{bmatrix} R_{r,r}(0) & R_{r,r}(-1) & \cdots & R_{r,r}(1-M) \\ R_{r,r}(1) & R_{r,r}(0) & \cdots & R_{r,r}(2-M) \\ & & \ddots & \\ R_{r,r}(M-1) & R_{r,r}(M-2) & \cdots & R_{r,r}(0) \end{bmatrix}.$$

Clearly, when $p = 2$, i.e., for Gaussian distributed signals, the expression for the covariation matrix is reduced to the well-known form of the covariance matrix. Hence, the source wavelet vector can be obtained from (18) with inversion techniques such as singular value decomposition algorithm.

## IV. Test Results and its Analysis

In this section, computer simulations are conducted to verify the performance of the proposed wavelet estimation method. The simulations are given in two parts: In the first part, two kinds of wavelets are estimated from two synthetic seismic traces, respectively, and in the second part, the wavelet is estimated from real seismic data.

### A. Synthetic Data

There are two groups of synthetic traces, illustrated in Fig. 1, computed as convolution results of a normalized $S\alpha S$ random vector with two types of wavelets, respectively. The normalized $S\alpha S$ random vector, used as pseudoreflectivity coefficients, generated with $\alpha = 1.8$, is illustrated in Fig. 2.

The pseudoreflectivity coefficients were generated by using the Chambers's method with the following steps [21].

Step 1) Generate $U$ uniform on $(-(1/2\pi), (1/2\pi))$ and $V$ exponential with mean 1.

Step 2) Compute $X = (\sin(\alpha U)/[\cos(U)]^{1/\alpha})[\cos(U - \alpha U)/V]^{(1-\alpha)/\alpha}$.

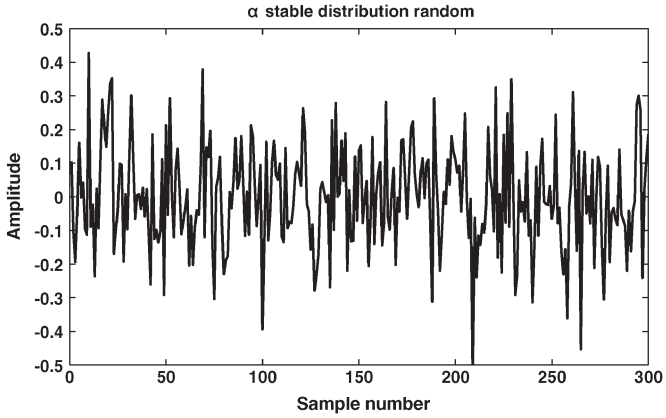


Fig. 2. $S\alpha S$ pseudoreflectivity coefficient with $\alpha = 1.8$.

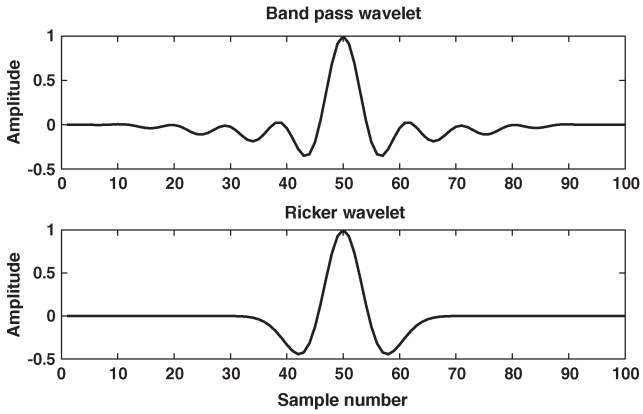


Fig. 3. Two types of wavelets. (a) Bandpass wavelet. (b) Ricker wavelet.

Step 3) Generalize scale and location $Y = \gamma^{1/\alpha}X + \mu$.

Step 4) Compute $\mathbf{r} = (Y/2 \times \max|Y|)$, where $\mathbf{r}$ is the pseudoreflectivity coefficient.

Two kinds of used true wavelets are illustrated in Fig. 3: The aforementioned one in the figure is a bandpass wavelet with a low-pass frequency of 10 Hz and a high-pass frequency of 50 Hz, and the other one is a Ricker wavelet with a center frequency of 40 Hz. The length of the wavelets is 100 samples.

Applying the proposed covariation method, the simulation work is to extract wavelets from the synthetic traces illustrated in Fig. 1 and the pseudoreflectivity coefficient illustrated in Fig. 2. In the following experiments, the length of the wavelets is 100 samples according to the given true wavelet length.

It is known that, for non-Gaussian $\alpha$-stable distributions, only moments less than characteristic $\alpha$ are finite. In particular, $\alpha$-stable distribution with $\alpha < 2$ does not have the second-order moment. The moment is an important parameter of the covariation method; in the following experiments, we set moments $p = 1.6$, 2.0, and 1.2, respectively. Note that, when $p = 2.0$, the covariation method is reduced to the well-known Gaussian covariance method. The extracted bandpass wavelets with different moments are shown in Fig. 4, and the amplitude spectrums of the wavelets are shown in Fig. 5. The estimated Ricker wavelets and their amplitude spectrums are shown in Figs. 6 and 7, respectively. The wavelets and their amplitude spectrums are plotted with different types of lines in the figures. From Figs. 4, 5, 6, and 7, it can be seen that,

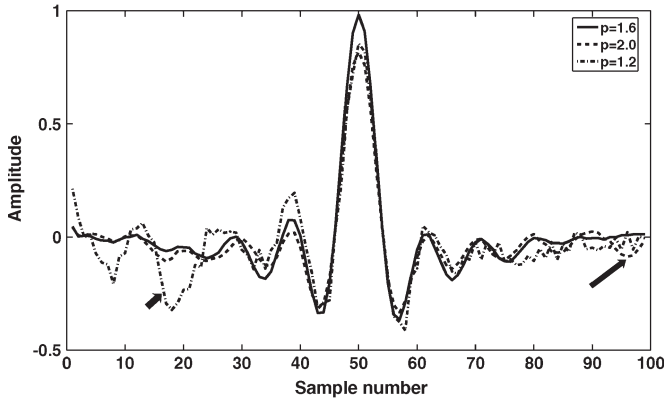


Fig. 4. Estimated bandpass wavelets with different moments.

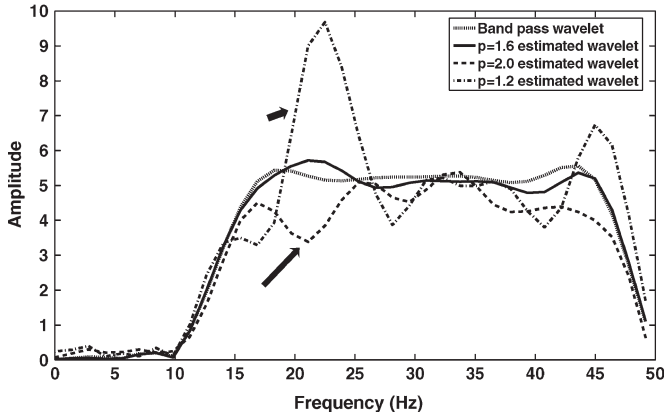


Fig. 5. Amplitude spectrums of bandpass wavelets with different moments.

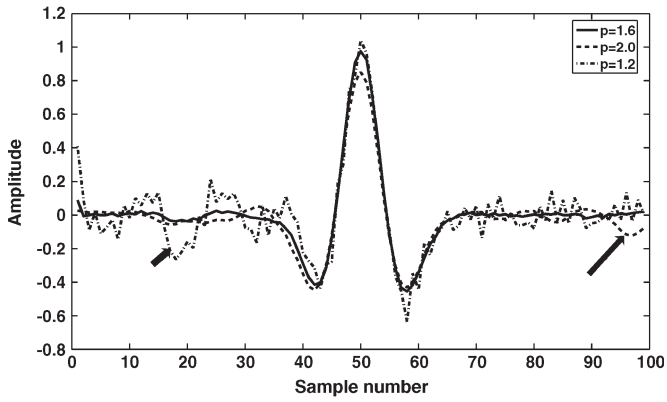


Fig. 6. Estimated Ricker wavelets with different moments.

when moment $p = 1.6$, the best wavelet is obtained in both experiments. As shown in Figs. 4 and 6, the waveforms of the extracted wavelets with the covariation method (when $p = 1.6$ and 1.2) are better than the wavelets extracted with the Gaussian covariance method (when $p = 2.0$). The unreasonable parts of the extracted wavelets with the Gaussian covariance method are marked with short arrows in Figs. 4 and 6, respectively. One will find an interesting phenomenon that the results with $p = 1.6$ are better than the results with $p = 1.2$, especially at the tail of the wavelets, marked with long arrows in Figs. 4 and 6, respectively. Due to the bad waveform, the wavelets with the Gaussian covariance method tend to have the roughest

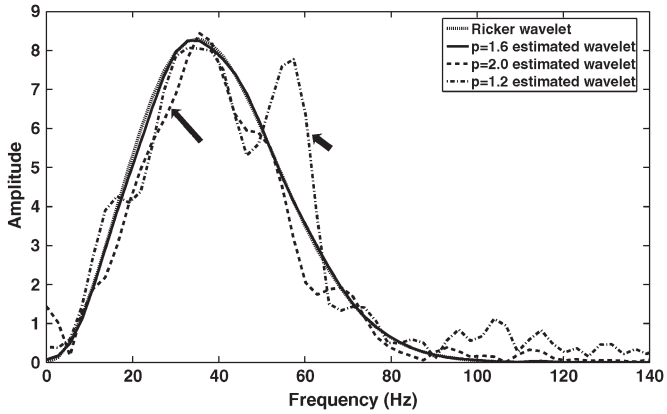


Fig. 7. Amplitude spectrums of Ricker wavelets with different moments.

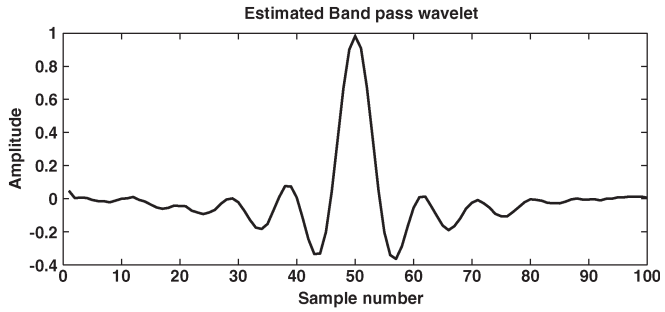


Fig. 8. Estimated bandpass wavelet.

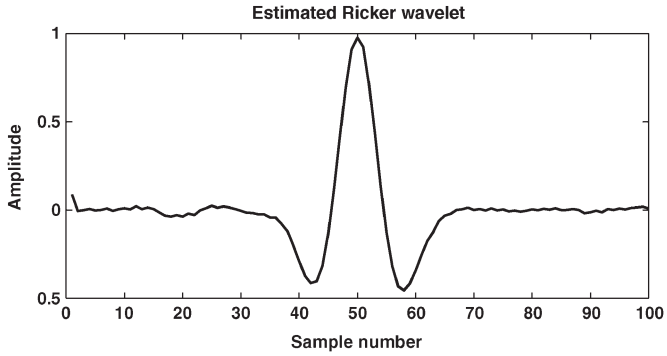


Fig. 9. Estimated Ricker wavelet.

amplitude spectrums. The unreasonable parts of the amplitude spectrums are marked with arrows in Figs. 5 and 7. The wavelet with $p = 1.6$ has a good waveform and a smooth amplitude spectrum that is close to the true wavelets. A conclusion may be generalized from the figures that the covariation method ($p < 2$, non-Gaussian $\alpha$-stable distribution) is more excellent than the covariance method ($p = 2$, Gaussian distribution).

The best recovered bandpass wavelet and Ricker wavelet (with moment $p = 1.6$) are illustrated in Figs. 8 and 9, respectively. As mentioned previously, the recovered bandpass wavelet and Ricker wavelet are in very good agreement with the true bandpass wavelet and Ricker wavelet, respectively. Fig. 10 shows the amplitude spectrums of the true bandpass wavelet (solid line) and its estimated wavelet (dashed line). It is clearly shown that the true and estimated wavelets have the same bandwidth, although they are slightly different toward the top of the spectrum curves due to estimation errors. The same

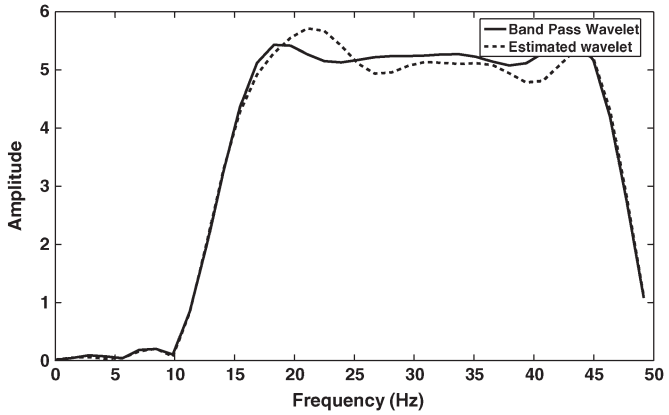


Fig. 10. Amplitude spectrums of the bandpass wavelet and its estimation wavelet.

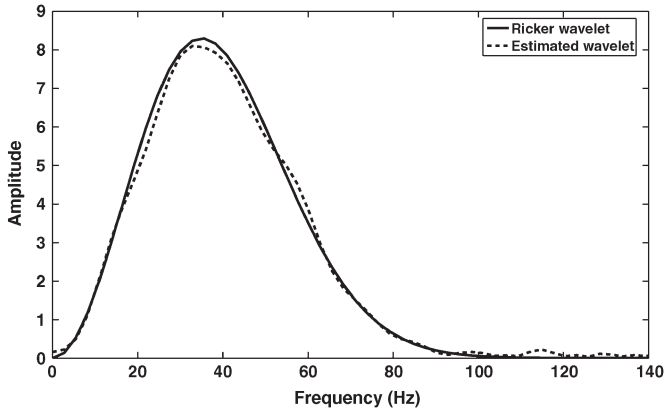


Fig. 11. Amplitude spectrums of the Ricker wavelet and its estimation wavelet.

conclusion can be made for the Ricker wavelet and its estimated wavelet, and the amplitude spectrums of the true Ricker wavelet (solid line) and recovered wavelet (dashed line) are shown in Fig. 11.

To ensure the validity of the recovered wavelets, synthetic trace error analysis involving recovered wavelets is conducted. Fig. 12(a) is a synthetic trace, generated by convolving the pseudoreflectivity coefficient shown in Fig. 2 with the true bandpass wavelet, tagged Syn1. Fig. 12(b) is a synthetic trace generated by convolving the pseudoreflectivity coefficients with the recovered bandpass wavelet, tagged Sgn2. The aforementioned two traces Syn1 (solid line) and Syn2 (dashed line) are shown together in Fig. 12(c), where the dotted line corresponds to Syn2. Fig. 12(d) is the error trace between the two traces. Error may be due to misfit between the true and estimated wavelets. As might be expected, synthetic trace Syn2 generated by the recovered bandpass wavelet approximates to trace Syn1 closely, and the amplitude of the error trace is slight and negligible. The maximum error rate (absolute value of the error divided by Syn1) is less than 5.0%. It is also true for the recovered Ricker wavelet, as shown in Fig. 13. Syn1 is the original trace shown in Fig. 1(b), Syn2 is the synthetic trace generated by the recovered Ricker wavelet, Fig. 11(d) is the error trace between Syn1 and Syn2, and a similar conclusion is drawn that the synthetic trace error is negligibly small. All of

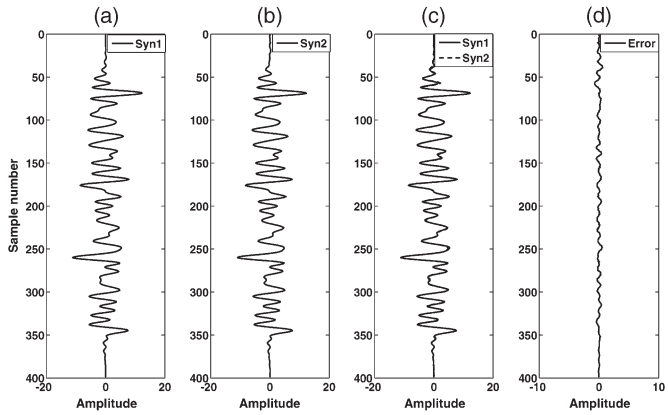


Fig. 12. Synthetic trace error analysis on the recovered bandpass wavelet. (a) Synthetic trace generated by the true bandpass wavelet. (b) Synthetic trace generated by the estimated bandpass wavelet. (c) Two synthetic traces. (d) Error of the two synthetic traces.

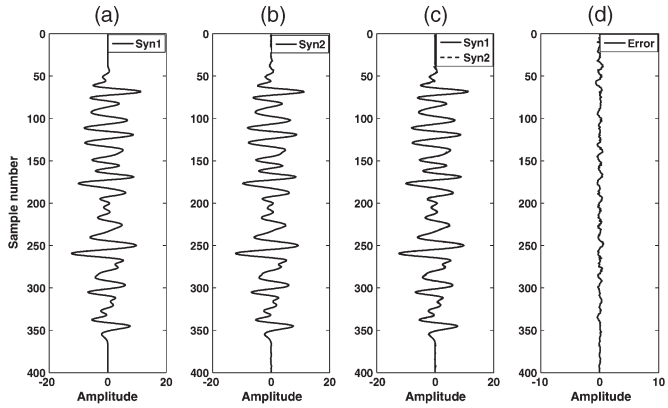


Fig. 13. Synthetic trace error analysis on the recovered Ricker wavelet. (a) Synthetic trace generated by the true Ricker wavelet. (b) Synthetic trace generated by the estimated Ricker wavelet. (c) Two synthetic traces. (d) Error of the two synthetic traces.

these evidences suggest that the recovered wavelet matches the true source wavelet well.

### *B. Test for Infinite Variance*

It is necessary to know whether the stable data distribution is Gaussian $(\alpha = 2)$ or non-Gaussian $\alpha$-stable $(0 < \alpha < 2)$. Since a property that differentiates the Gaussian and non-Gaussian stable distributions is that non-Gaussian stable distributions do not have a finite variance, such tests are called test for infinite variance. A general approach is to test that the distribution has a finite variance. Specifically, let $X_k$, $k = 1, \cdots, N$, be samples from the same stable distribution. For each $1 \leq n \leq N$ form, the unbiased sample variance based on the first $n$ observations is [10]

$$V_n^2 = \frac{1}{n-1} \sum_{k=1}^{n} (X_k - \overline{X}_n)^2$$

where

$$\overline{X}_n = \frac{1}{n} \sum_{k=1}^{n} X_k.$$

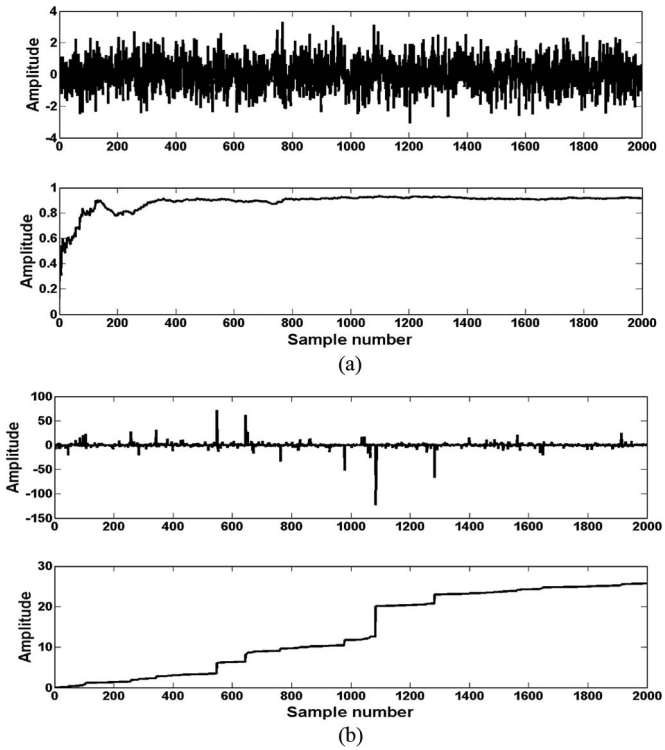


Fig. 14. Two sets of random $\alpha$-stable distributions and their running sample variances. (a) $\alpha = 2.0$. (b) $\alpha = 1.4$.

Moreover, plot the running sample variance estimate $V_n^2$ against $n$. If the data have a finite variance, $V_n^2$ should converge to a finite value. Otherwise, $V_n^2$ will diverge.

There are two sets of random $\alpha$-stable distribution samples generated for $\alpha = 2.0$ and 1.4; each has 2000 samples, applied to illustrate the effectiveness of this test. The random distributions and running sample variances are shown in Fig. 14. Note that, with only $\alpha = 2.0$ (Gaussian distribution), $V_n^2$ converges to a finite value.

### C. Characteristic $\alpha$ Estimation

In our proposed method, characteristic $\alpha$ plays a key role in moment choosing; however, the estimation of non-Gaussian $\alpha$-stable distributions is general severely hampered by the lack of known closed-form density functions. There was a useful suboptimal numerical method named sample quantile method first suggested by Fama and Roll [22] to estimate the characteristic $\alpha$. Moreover, McCulloch [23] developed the method to eliminate the asymptotic bias.

The quantile method is a simple and frequent way for rough estimation of the parameters of an $S\alpha S$ distribution with $1 \leq \alpha \leq 2$. Defining

$$v_\alpha = \frac{x_{0.95} - x_{0.05}}{x_{0.75} - x_{0.25}}.$$

In the aforementioned formula, $x_f$ denotes the $f$th population quantile, so that $f = F(x_f)$, where $F(x_f)$ is a distribution function, roughly estimated by the histogram of data in this paper. An estimate $\widehat{\alpha}$ can be obtained by searching a table of standard $S\alpha S$ distribution functions (see Holt's work [23]).

TABLE I
VALUES OF $v_\alpha$ AND $\alpha$

| $v_\alpha$ | 2.439 | 2.5 | 2.6 | 2.7 | 2.8 | 3.0 | 3.2 | 3.5 | 4.0 | 5.0 | 6.0 |
|---|---|---|---|---|---|---|---|---|---|---|---|
| $\alpha$ | 2.0 | 1.916 | 1.808 | 1.729 | 1.664 | 1.563 | 1.484 | 1.391 | 1.279 | 1.128 | 1.029 |

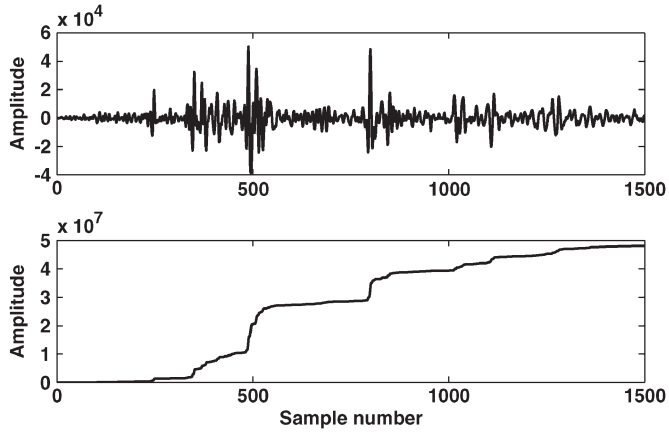


Fig. 15. Real seismic data and their running sample variance.

For $S\alpha S$, $\beta = 0$. An estimate $\widehat{\alpha}$ can be obtained by searching a table of standard $S\alpha S$ distribution functions. Table I is derived from McCulloc's tabulation [23].

### D. Real Data

A real field datum used to test the feasibility of the covariation wavelet extracting approach was collected from a survey in Southwest Sichuan, China. In the work of source seismic wavelet estimation, one well is used.

In the application of wavelet estimation, it is necessary to test that the seismic data are Gaussian or non-Gaussian $\alpha$-stable distributions. Fig. 15 shows the seismic data and their running sample variance. It can be seen that the real seismic data do not have a finite variance, and their running sample variance is similar to that of the non-Gaussian $\alpha$-stable distributions randomly shown in Fig. 14. It may be more logical to draw a conclusion that the real seismic is non-Gaussian than Gaussian.

Before extracting a wavelet, characteristic $\alpha$ of the seismic trace from the well location and reflectivity coefficient should be estimated. Using the estimation method from Section IV-C, the seismic trace and its histogram $H$ are shown in Fig. 16. If $f = \sum_{i=0}^{M} H(i)$, then $x_f = S(M)$, where $S(1) \leq S(2) \leq \cdots \leq S(N)$ is the ascending order of the seismic trace. Based on this method, one obtains $v_\alpha = 2.6250$. Searching Table I, the estimated characteristic of the seismic trace $\widehat{\alpha}_s \approx 1.7883$. Using the same computing method, it gets the characteristic of the reflectivity coefficient $\widehat{\alpha}_r \approx 1.8021$.

In this paper, the depth range of the section used for wavelet estimation is between 3971.75 and 5548.25 m. Fig. 17 shows that the seismic data correspond to the well, acoustic impedance, and reflectivity coefficient of the well, where the acoustic impedance is computed by well logs and the reflectivity coefficient corresponds to the computed acoustic impedance. Note that the seismic data shown in Fig. 17 are part of the one in Fig. 16.

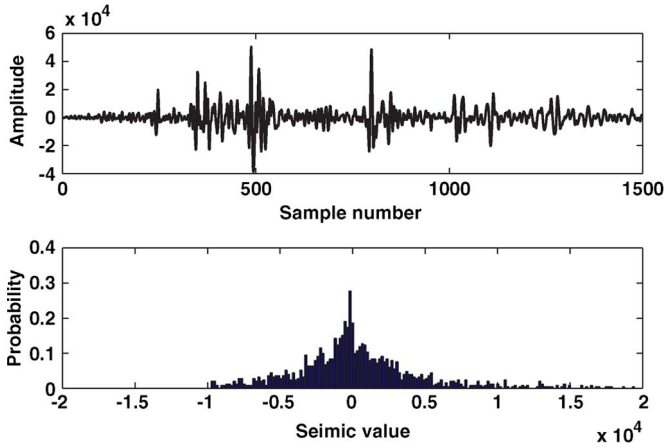


Fig. 16. Seismic trace and its histogram.

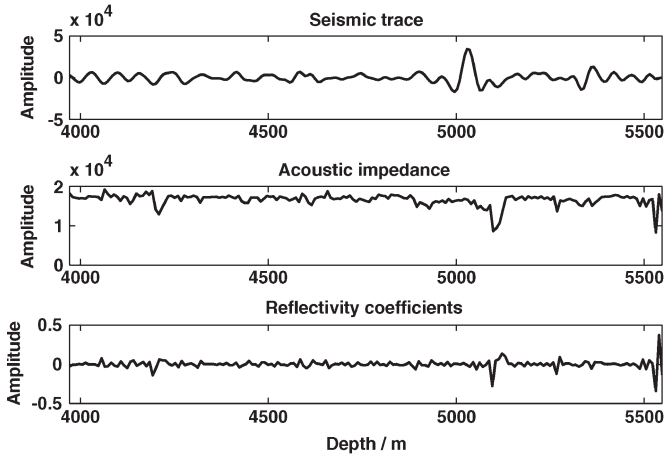


Fig. 17. Real data example.

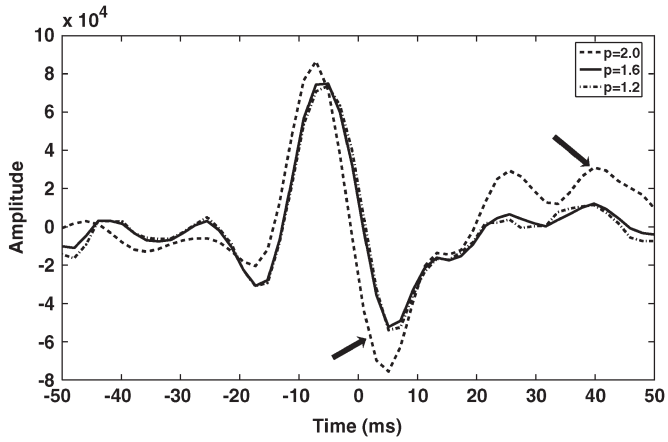


Fig. 18. Estimated wavelets from real data.

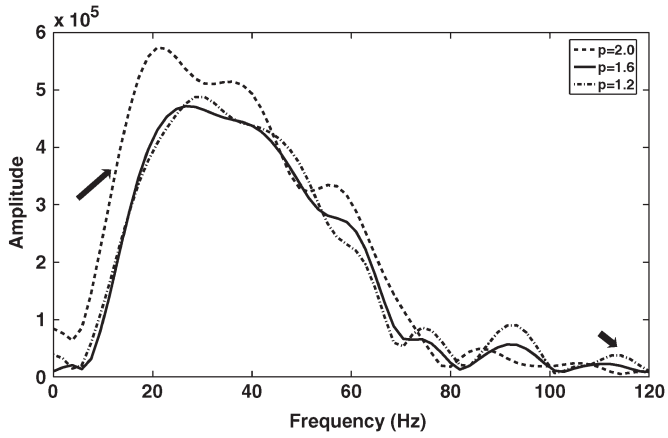


Fig. 19. Amplitude spectrums of the recovered wavelets from real data.

The length of the wavelet may influence the quality of the result. However, it is a hard work to decide a reasonable one. It is well known that the seismic wavelet is a representation of the explosive seismic source signal. Therefore, a wavelet should be short and should have a reasonable bandwidth. According to our experience, the length of the wavelet is set to 100 ms. The effect of statistical moments is also considered, setting moments $p = 2.0$, 1.6, and 1.2, respectively. As mentioned in Section III, covariation is reduced to Gaussian covariance when $p = 2.0$. Fig. 18 shows the recovered wavelets from these real data using the proposed covariation wavelet estimation method, and Fig. 19 shows the amplitude spectrums of the recovered wavelets. The waveforms and amplitude spectrums are shown with different lines. It can clearly be seen that the recovered wavelet with moment $p = 2.0$ is worse than the others, its waveform is unstable, and its amplitude spectrum is rough. The unreasonable parts are marked with long arrows in Figs. 18 and 19. The wavelet with moment $p = 1.6$ is similar to the one with moment $p = 1.2$; however, the latter has an unreasonably stronger high frequency, marked with a short arrow in Fig. 19.

It is well known that synthetic trace error analysis is a common way to check whether the recovered wavelet matches the real source wavelet or not. If the recovered wavelet matches the source wavelet well, the amplitude of the error trace between the real seismic trace and the synthetic trace generated by convolving the recovered wavelet with the reflectivity coefficient should be small enough. The wavelet recovered with moment $p = 1.6$ is taken for synthetic trace error analysis. Fig. 20(a) shows the real seismic trace tagged as S1 and the synthetic trace tagged as S2, and Fig. 20(b) is the error ratio between the real trace and the synthetic trace. It can be seen that S2 and S1 are very close to each other near the greatest central peak, while the misfit tends to increase toward the ends of the trace owing to the convolution truncation error. Note that there is no truncation effect in the synthetic data wavelet estimation experiments as traces Sy1 and Sy2 are generated by convolving the same reflectivity coefficients; however, in the real seismic wavelet estimation case, only synthetic trace S2 is generated by convolving the reflectivity coefficients with the estimation wavelet. Generally, the maximum error rate (absolute value of the error divided by S1) is less than 8.0%.

From both synthetic and real data experiments, it can be seen that the order of the moment $p$ is an important parameter for the wavelet estimation. For non-Gaussian $\alpha$-stable distributions, the moment $p$ must be less than characteristic $\alpha$. However, if the moment is too small, the estimated result may be bad. According to our experience, the reasonable value of the moment should be less than the characteristic but near to the characteristic. Taking the real data wavelet estimation, for

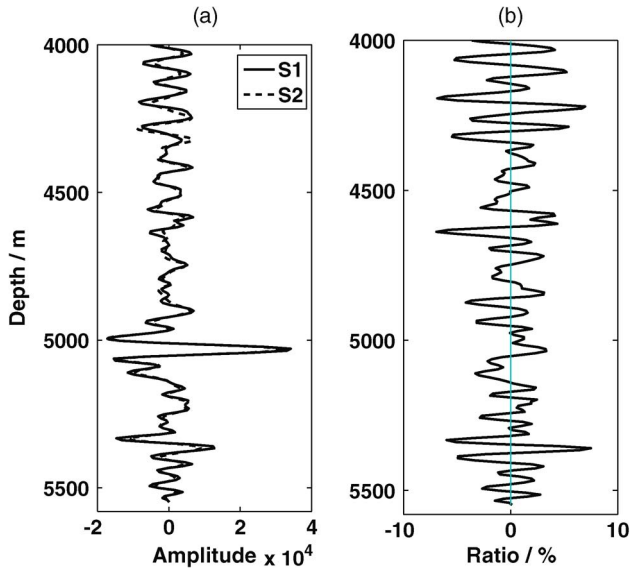


Fig. 20. Synthetic trace error analysis.

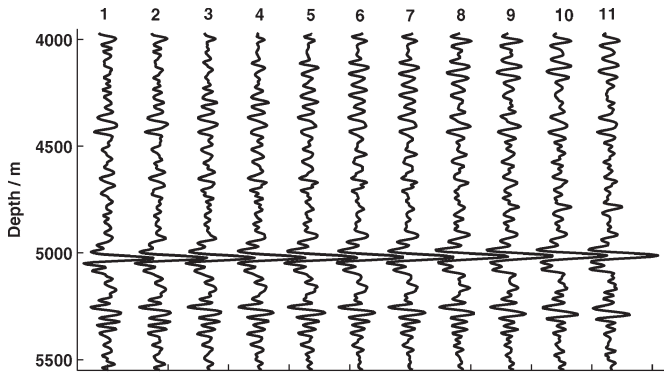


Fig. 21. Real seismic traces.

example, as the estimated characteristic of the seismic trace is $\widehat{\alpha}_s \approx 1.7883$, the moment $p = 1.6$ is better than $p = 2.0$ (Gaussian) and $p = 1.2$. Therefore, it is strongly suggested that one conducts the characteristic estimation before wavelet extraction.

In the previous experiments, the wavelets were extracted by a single seismic trace. To test the feasibility of the proposed covariation wavelet estimation method, a portion of the real seismic data near the well location, as shown in Fig. 21, was used for wavelet estimation. The depth range of the seismic traces is also between 3971.75 and 5548.25 m, and they are thought to have the same statistic characteristics. In this example, the length of the wavelet is set to 100 ms, and the moment is set to $p = 1.6$. Fig. 22 shows the inversion result of the 11 traces in Fig. 21. It can be seen that every estimated wavelet has a great central peak and the waveforms extracted from different traces are very consistent. This illustrates the stability of the extraction approach proposed in this paper.

### *E. Real Data Inversion*

In this section, the estimated wavelet was applied in seismic acoustic impedance inversion. The impedance section, obtained trace by trace using the FLOM inversion method [9], is shown

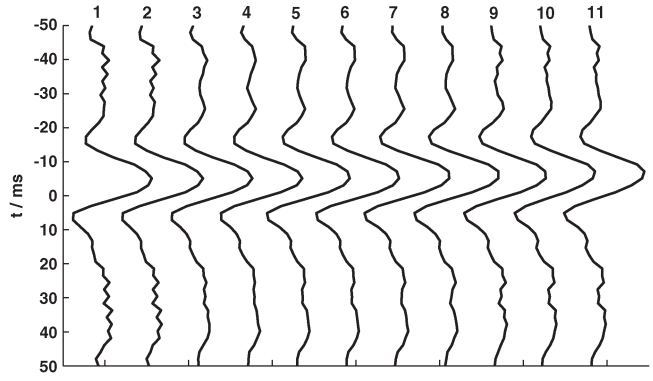


Fig. 22. Estimated wavelets from real traces.

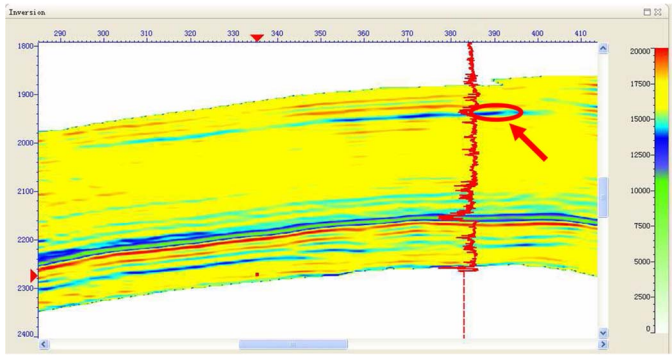

Fig. 23. Acoustic impedance inversion result.

in Fig. 23. It shows a great continuity and resolution detail in the highlighted zone. We believe that any interpretation carried out on the high-resolution impedance section is bound to be accurate. For example, according to the well log interpretation, there is a gas reservoir with a time range of 1900–2240 ms. The reservoir clusters are clearly seen in the impedance section; they are marked with a red ellipse in Fig. 23. The inversion result demonstrates the validity of the covariation wavelet estimation method.

## V. Conclusion

This paper has proposed a new wavelet estimation approach based on the non-Gaussian $\alpha$-stable distribution, under the assumption that seismic signals follow a non-Gaussian $\alpha$-stable distribution. Consequently, only moments of order less than characteristic exponent $\alpha$ are finite, and the wavelet estimation algorithm should be conducted with covariation based on the principle of FLOM rather than covariance. This method is more stable than the traditional Gaussian method (when the characteristic is 2).

Tests using both synthetic data and real seismic data are conducted to verify the performance of the proposed method. In the synthetic data inversion experiment, the recovered Ricker wavelet and bandpass wavelets are close to the theoretical wavelets, respectively.

In the real seismic data inversion case, the sample quantile method was applied in estimating the characteristic of real seismic data and the wavelet estimated with different moments.

The results show that the reasonable moment should be less than the characteristic but close to the characteristic.

These experimental results not only demonstrate the viability of the covariation wavelet estimation approach described here but also show the reliability of the FLOM model. As Gaussian distribution is a special case of $\alpha$-stable distribution, the proposed method is suitable for Gaussian cases.

## REFERENCES


[1] E. A. Robinson, "Predictive decomposition of seismic traces," *Geophysics*, vol. 22, no. 4, pp. 767–779, Oct. 1957.

[2] V. B. Mirko and D. T. Pham, "Robust wavelet estimation and blind deconvolution of noisy surface seismic," *Geophysics*, vol. 73, no. 5, pp. V37–V46, Sep./Oct. 2008.

[3] B. B. Yue, Z. M. Peng, Y. G. Hong, and W. Zou, "Wavelet inversion of pre-stack seismic angle-gather based on particle swarm optimization algorithm," *Chin. J. Geophys.*, vol. 52, no. 12, pp. 3116–3123, Dec. 2009.

[4] X. Lv and Y. Wang, "Mixed-phase wavelet estimation by iterative linear inversion of high-order statistics," *J. Geophys. Eng.*, vol. 4, no. 2, pp. 184–193, Jun. 2007.

[5] W. Lu, Y. Zhang, S. Zhang, and H. Xiao, "Blind wavelet estimation using a zero-lag slice of the fourth-order statistics," *J. Geophys. Eng.*, vol. 4, no. 1, pp. 24–30, Mar. 2007.

[6] H. Sun, Y. Dai, S. Wang, and P. Xing, "Research on the high-efficiency ARMA model applied in seismic wavelet estimation," in *Proc. IEEE 10th Int. Conf. Signal Process.*, 2010, pp. 164–167.

[7] A. T. Walden, "Non-Gaussian reflectivity, entropy, deconvolution," *Geophysics*, vol. 50, no. 12, pp. 2862–2888, Dec. 1985.

[8] B. Godfrey and J. F. Claerbout, "Two methods of deconvolution: Power spectrum smoothing and parsimonious deconvolution," Stanford Exploration Project, Stanford, CA, USA, SEP-14, pp. 207–226, 1978.

[9] B. Yue, Z. Peng, and Q. Zhang, "Seismic inversion method with $\alpha$-stable distribution," *Chin. J. Geophys.*, vol. 55, no. 4, pp. 1307–1317, 2013.

[10] M. Shao and C. L. Nikias, "Signal processing with fractional lower order moments: Stable processes and their applications," *Proc. IEEE*, vol. 81, no. 7, pp. 986–1010, Jul. 1993.

[11] C. L. Nikias and M. Shao, *Signal Processing With Alpha-Stable Distributions and Application*. New York, NY, USA: Wiley, 1995.

[12] J. Wang, E. E. Kuruoglu, and T. Zhou, "Alpha-stable channel capacity," *IEEE Commun. Lett.*, vol. 15, no. 10, pp. 1107–1109, Oct. 2011.

[13] X. Y. Ma and C. L. Nikias, "Parameter estimation and blind channel identification in impulsive signal environments," *IEEE Trans. Signal Process.*, vol. 43, no. 12, pp. 2884–2897, Dec. 1995.

[14] M. Rupi, P. Tsakalides, C. L. Nikias, and E. Del Re, "Robust constant modulus arrays based on fractional lower-order statistics," in *Proc. IEEE Int. Conf. Acoust., Speech Signal Process.*, 1999, vol. 6, pp. 2945–2948.

[15] T. H. Liu and J. M. Mendel, "A subspace based direction finding algorithm using fractional lower order statistics," *IEEE Trans. Signal Process.*, vol. 49, no. 8, pp. 1605–1613, Aug. 2001.

[16] P. Tsaklides and C. L. Nikias, "The robust covariation-based MUSIC (ROC-MUSIC) algorithm for bearing estimation in impulsive noise environment," *IEEE Trans. Signal Process.*, vol. 44, no. 7, pp. 1623–1633, Jul. 1996.

[17] A. Buland and H. More, "Bayesian wavelet estimation from seismic and well data," *Geophysics*, vol. 68, no. 6, pp. 2000–2009, Nov./Dec. 2003.

[18] L. Tenorio, "Modeling non-Gaussian reflectivities: Generalizing Wiener–Levison deconvolution," *Geophysics*, vol. 66, no. 6, pp. 1913–1920, Nov. 2001.

[19] W. H. Liu, Y. Y. Wang, and T. S. Qiu, "Evoked potential delay estimation by using covariation correlation approach," in *Proc. 2th Int. Conf. Bioinform. Biomed. Eng.*, 2008, pp. 625–655.

[20] A. M. Hmidat and M. A. S. Hassan, "Nonlinear DOA estimation for CDMA system in impulsive wireless channels," in *Proc. 7th Int. Symp. Wireless Commun. Syst.*, 2007, pp. 431–435.

[21] J. M. Chambers, C. L. Mallows, and B. W. Stuck, "A method for simulating stable random variables," *J. Amer. Statist. Assoc.*, vol. 71, no. 354, pp. 340–344, Jun. 1976.

[22] E. F. Fama and R. Roll, "Parameter estimation for symmetric stable distributions," *J. Amer. Statist. Assoc.*, vol. 66, no. 334, pp. 331–338, Jun. 1971.

[23] D. R. Holt and E. L. Crow, "Tables and graphs of the stable probability density functions," *J. Res. Natl. Bureau Standards—B. Math. Sci.*, vol. 77B, no. 3/4, pp. 143–198, Jul.–Dec. 1973.


**Bibo Yue** received the B.S. degree in electronic and information engineering from Hubei University, Wuhan, China, in 2007 and the M.S. degree in signal and information processing from the University of Electronic Science and Technology of China, Chengdu, China, in 2010, where he has been working toward the Ph.D. in signal and information processing since 2010.

His research interests include non-Gaussian seismic inversion and evolutionary computing.

**Zhenming Peng** received the Ph.D. degree in earth exploration and information technology from Chengdu University of Technology, Chengdu, China, in 2001.

He is currently a Professor with the University of Electronic Science and Technology of China, Chengdu. His research interests include image processing, radar signal processing, and target recognition and tracking.

Dr. Peng is a member of the IEEE and the Aerospace Society of China.

**Qiheng Zhang** received the B.S. degree in television major from the University of Electronic Science and Technology of China (UESTC), Chengdu, China, in 1977. His research interests include photoelectric detection, digital image processing, and target detection.